

Compositional zoning in sphalerite crystals

FRANCESCO DI BENEDETTO,^{1,*} GIAN PIERO BERNARDINI,² PILAR COSTAGLIOLA,³ DAVID PLANT,⁴
AND DAVID J. VAUGHAN⁴

¹Museo di Storia Naturale, Università di Firenze, via G. La Pira, 4-150121, Firenze, Italy

²Piazzale Donatello 18, I-50132, Firenze, Italy

³Dipartimento di Scienze della Terra, Università di Firenze, via G. La Pira, 4-150121, Firenze, Italy

⁴Department of Earth Sciences, University of Manchester, Oxford Road, H13 9PL, Manchester, U.K.

ABSTRACT

A series of natural sphalerite samples, characterized by an inhomogeneous (zonal) distribution of Fe, Mn, and Cd atoms substituting for Zn, has been investigated by electron probe microanalysis and X-ray element distribution mapping. The cation distributions are markedly inhomogeneous due to the reciprocal effects of the minor elements on their respective solubilities. In particular, zonal partitioning between Fe and Mn and between both cations and Hg was observed in sphalerite, as well as coupled Cu-In and Cu-Fe substitutions. Distinctly different distribution patterns were identified in Mn-free samples with a low Fe-content, as compared to Mn-bearing samples. In the former case, Fe and Cd distribution patterns are very similar, whereas in the latter case, Cd is distributed homogeneously and Mn and Fe patterns are antithetic. The different oscillatory zoning observed in Mn-free samples is attributed to a fast, self-organized solute (Fe, Cd) deposition, although an alternative external origin cannot be ruled out. On the other hand, in the presence of Mn, zoning may be related to an absorption process at the mineral-fluid interface controlled by a competition between Mn and Fe that may explain the observed limited coupled concentration of these elements in sphalerite. The homogeneous distribution of Cd suggests relatively slow crystal growth.

INTRODUCTION

Sphalerite, the cubic polymorph of ZnS, exhibits a wide range of compositional variations in natural specimens (e.g., Patrick et al. 1993, 1998; Axelsson and Rodushkin 2001) where other metal cations can replace Zn in the tetrahedral site. One consequence is that sphalerite is the major source not only of Zn, but also of Cd, In, Ge, and Ga. The concentration of such impurities in sphalerite is relevant to ore-processing technology, greater knowledge potentially improving the recovery of both Zn and the secondary products. In addition, sphalerite is of technological interest as a II-VI semiconductor, particularly because of its wide band-gap. This band gap may be adjusted or tuned by replacing an appropriate number of Zn atoms by other cations with interesting paramagnetic properties, such as Fe, Mn, and Co, producing the so-called Diluted Magnetic Systems, DMS [e.g., see Furdyna (1988) for Mn-based DMS and Twardowski (1990) for Fe-based DMS].

In many sphalerite crystals, the extent of substitution of Zn by other cations can vary throughout the crystal, with the development of discrete compositional bands of widths that range in scale from centimeters to micrometers. Coupled substitution mechanisms (e.g., Cu+In for Zn) are responsible for the more unusual banded sphalerites, found only in few localities, and in ores important for the recovery of In and Ge (Johan 1988; Kieft and Damman 1990; Patrick et al. 1993). The refractory behavior of sphalerite has been well documented (Craig and Vaughan 1994; Lepetit et al. 2003, and references therein), and

the compositional variations in banded crystals are commonly believed to reflect physico-chemical variations that took place during crystal growth, rather than post-depositional re-equilibration processes (although with some exceptions; e.g., Roedder and Dwornik 1968). Provided that the precipitation of sphalerite has taken place in equilibrium with a suitable buffering mineral assemblage, the composition of the sphalerite may be used as an indicator of formation conditions (e.g., Scott 1973; Cook 1996). Similarly, any compositional zoning may be used as a tool to reconstruct the evolution of the physico-chemical conditions in the precipitating fluid during crystal growth.

Because of its petrological applications, compositional zoning in minerals has been studied extensively in recent years. In particular, an increasing number of authors have pointed out that zoning reflects self-organized non-equilibrium processes that may occur, under particular circumstances, during crystal growth (Ortoleva 1990; Reeder et al. 1990; Sultan et al. 1990; L'Heureux 1993; Holten et al. 1997, 2000; Katsev and L'Heureux 2001; L'Heureux and Jamtveit 2002). Holten et al. (1997) recognized two main mechanisms responsible for compositional zoning: "external" processes related to large-scale variations of mineralizing fluid composition in open systems; and "internal" processes taking place, at a smaller scale, in systems that can be considered closed. The internal processes are characterized by self-organized phenomena that may arise as a consequence of fluctuations, instability, chaotic behavior, and evolutionary trends that have been observed not only in mineralogy, but also in other fields such as physics, chemistry, biology, and environmental sciences (Bjørkum and Walderhaug 1990; Chadam and Ortoleva 1990; Walgraef 1990; Wei and Ortoleva 1990; Dewers

* E-mail: dibenefr@geo.unifi.it

and Ortoleva 1994; Prigogine 1997; L'Heureux 1993; Shore and Fowler 1996; Holten et al. 1997, 2000; Katsev and L'Heureux 2001; L'Heureux and Jamtveit 2002). Such mechanisms have been considered responsible for the compositional banding observed in a variety of minerals, including sphalerite. Many studies (Oen et al. 1980; L'Heureux 1993; Patrick et al. 1993; L'Heureux 2000; Katsev and L'Heureux 2001) have shown that two (or more) different cations may compete for incorporation into a structural site during the crystallization of a mineral, inducing the preferential incorporation of one cation while the other cation concentrates in the fluid at the crystal interface (provided that renewal of the mineralizing fluid around the growing crystal is slow enough). The excluded cation starts being incorporated when its concentration rises over a given threshold, following a typical feedback reaction pathway (L'Heureux 1993; Dewers and Ortoleva 1994; Katsev and L'Heureux 2001). Feedback processes, produced by competing mechanisms during crystal growth, represent a self-organized control on the composition of the fluid at the crystal-fluid interface and, consequently, on mineral zoning.

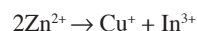
A further form of compositional zoning in crystals that may be ascribed to self-organization phenomena is sector zoning. This mechanism implies compositional differences among time-equivalent zones of crystallographically non-equivalent faces, as reported by Vesselinov and Kerestedjian (1995). Sector zoning is observed in minerals as a function of out-of-equilibrium, kinetically controlled factors, such as the surface atomic arrangements of the growing phases and rapid growth rates (Vesselinov and Kerestedjian 1995; Agrosi et al. 2002). However, Watson et al. (1995) developed a numerical model according to which sector zoning may also occur during equilibrium crystal growth under specific boundary constraints.

In the mineral sphalerite, Bernardini et al. (2004) have shown evidence of Mn cluster formation in natural samples using EPR spectroscopy. To investigate this inhomogeneous distribution of minor elements, and to relate them to the origin of the sphalerite, the present investigation of natural sphalerite samples has been undertaken using accurate Electron Probe Micro-Analysis (EPMA). Recent studies (Kojonen and Johanson 1999) have pointed out the advantages of this technique, widely used because of its very small spot size during analysis (down to 1 μm^2) and capability of detecting trace elements in the ppm range. The present study was carried out on sphalerite crystals from different ores to determine the metal concentrations and their distributions. The study followed a phenomenological approach, i.e. using zoned crystals of sphalerite and assuming that their banding is primary, acquired during crystal growth from a fluid independently of the minerogenic context. The proposed competition between Mn and Fe for the replacement of Zn, its possible relationship to an "internally" controlled zoning mechanism during crystal growth, and the role of Cd have been investigated through the utilization of accurate Mn-Fe-Cd distribution maps.

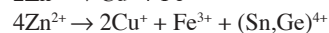
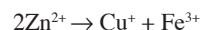
Major, minor, and trace element distributions in ZnS

Scott and Barnes (1972) stated that the solubilities of Fe, Cd, and Mn are greater in the hexagonal ZnS polymorph, wurtzite, than in sphalerite, which, in turn, is stable even if extensively substituted by different metals. In particular, in natural occur-

rences, FeS has been found to replace ZnS (in sphalerite) by up to 56 mol% (Balabin and Urusov 1995; Patrick et al. 1998) whereas CdS concentrations are definitely lower (<14 mol%, Tauson et al., 1977; Maurel, 1978). Iron and Cd are ubiquitous substituents in sphalerite and are found in almost all sphalerite ores, even if only in small amounts, whereas Mn has been found only in certain ores at up to 15 mol% MnS (Patrick et al. 1998). Furdyna (1988) suggested a lower concentration limit (10 mol%), with the wurtzite structure being stabilized at higher Mn-contents. As regards other divalent cations, such as Co and Ni, no significant amounts have been observed in natural sphalerite specimens (Axelsson and Rodushkin 2001; Huston et al. 1995; Rager et al. 1996), even though CoS replacement for ZnS may reach 20 mol% in synthetic samples (Hall 1961; Lawniczac-Jablonska et al. 1994). Copper and Indium do not often occur in a divalent state in sulfides and sulfosalts (Bente 1987; Patrick et al. 1993; Di Benedetto et al. 2002). According to Johan (1988), Cu and In may replace Zn through a coupled mechanism:



forming band-shaped roquesite (CuInS_2) domains. These bands, characterized by different colors, may be recognized easily in sphalerite crystals by means of optical microscopy (Patrick et al. 1993). Coupled and/or multiple substitutions may also account for the high Cu-, Sn-, and Ge-contents observed in some sphalerite crystals (Wiggins and Craig 1980; Hutchinson and Scott 1981; Johan 1988) through mechanisms such as:



Many studies have been dedicated to the determination of binary, ternary, and quaternary phase relations involving sphalerite and the important binary sulfides, pointing to the capability of this mineral to host even larger amounts of minor-substituting elements under high-pressure and high-temperature conditions. In particular, the FeS content may increase up to 60 mol% with increasing temperature (Barton and Toulmin 1966; Balabin and Urusov 1995), whereas CdS and MnS are observed at up to 20 mol% under high temperature and/or pressure (Tauson and Chernyshev 1977; Tauson et al. 1977). The maximum Ni-content has been established to be 1.16 mol%, increasing up to 1.4 mol% in the absence of Fe (Czamanske and Goff 1973)

Some authors (e.g., Furdyna 1988; Twardowski 1990) have discussed a possible inhomogeneous distribution of paramagnetic cations replacing Zn in sphalerite, usually assumed to be distributed randomly. Balabin and Sack (2000) observed the thermodynamic stabilization of pairs and small clusters of Fe, in agreement with Twardowski et al. (1988). On the other hand, Tauson and Chernyshev (1977) proposed a model involving a quasi-ideal solid solution involving ZnS and the main substituting elements (Fe, Mn, and Cd). These considerations lead to questions about possible mutual interactions between Zn and these substituting elements and between the substituting elements themselves.

EXPERIMENTAL PROCEDURES

Table 1 lists the analyzed sphalerite specimens with their provenance. The samples ranged in color from pale yellow to reddish-orange to black. Eighteen of

the samples are from the collections of the Natural History Museum, University of Florence, whereas samples SPEH1 and 22551 are from the Department of Earth Sciences, University of Manchester. All specimens were single crystals, or chips from larger single crystals. They were embedded in an epoxy resin, polished with diamond paste down to $\frac{1}{4}$ μm and analyzed by means of a CAMECA SX100 Electron Microprobe at Manchester. Experimental conditions were chosen to maximize the peak-to-background ratio and to avoid possible interferences arising from partially overlapping X-ray emission peaks. Particular care was taken to achieve low detection limits, through an analytical CAMECA programme devoted to trace-element analysis. These limits can be as low as a few parts per million, provided that the mineral is stable enough to withstand the high beam voltages and currents necessary. Point analyses were performed at 25 kV and 20 nA for major elements, and at 25 kV and 100 or 200 nA for minor or trace elements. Counting times, ranging from 20 s for major and 50–100 s for minor/trace elements, were chosen so as to balance improved counting statistics against the total time taken for a single analysis (usually 600 s), to reduce the damage to the samples under an electron beam of 5 μm diameter. Synthetic ZnS (for Zn and S), ZnSe (for Se), and GaAs (for Ga and As), natural pyrite (for Fe), cinnabar (for Hg), chalcocopyrite (for Cu), and the metals themselves for V, Ti, Cr, Mn, Co, Ni, Cd, Sn, and Ge were used as standards. Peak positions and background levels were calibrated using the X-ray emission peaks of the standards. Raw X-ray intensity values were ZAF corrected using the CAMECA software (Ancy et al. 1980). Potential errors arising from the comparison of the peak intensities of the trace elements with those of the standards, where such elements are abundant, were reduced by using a set of standards with very similar characteristics (nature of chemical bonding, crystal structure) to minimize matrix effects. Nevertheless, the choice of the standards was dictated by the need to improve the peak-to-noise ratio and the stability of the X-ray emission of the standard peaks. The mean detection limits provided by the software are reported in Table 2, in addition to the X-ray line and analyzing crystals used. These detection limits are in good agreement with the results provided by Fialin et al. (1999) and they are similar to those obtained by Axelsson and Rodushkin (2001), using Laser Ablation Inductively Coupled Plasma Mass Spectrometry (LA-ICP-MS). These authors applied this technique to the analysis of trace elements in sphalerite, determining Mn-, Co-, and Cu-contents down to 20 ppm. At least ten point analyses were collected for each sample. Eleven samples in which only Fe, Mn, and Cd were detected by EPMA, as minor vicariants, were chosen for X-ray mapping. The experimental conditions used were a beam current of 200 nA, an accelerating voltage of 25 kV, and a nominal 1 μm diameter beam spot. An area of 1.5 \times 1.5 mm was covered by a 512 \times 512 pixel grid, the pixel step being 3 μm . FeK α and MnK α lines were measured simultaneously using two different LIF crystals, whereas the CdL α line was recorded using a PET crystal. Comparison with the results of point analyses on the same samples allowed a minimum detection limit of \sim 0.1 wt% for each element, counting times being 0.025 s per pixel.

RESULTS

The mean values of major-, minor-, and trace-element concentrations are reported in Tables 3 and 4, respectively. The

low analytical totals (Table 3), spread around a value of \sim 98 wt%, are probably due to a slightly different carbon coating between standards and samples, as confirmed by the small range of the data, all of which lie within \pm 1.5 wt% and most within a much smaller range. The sum of metal cation contents (ΣMe) vs. S contents has been evaluated for each point analysis, to check the stoichiometry and the overall quality of the data (Fig. 1). The small deviation of analytical points from the ideal 1:1 ratio is similar to the total analytical error.

For the mean data shown in Table 3, only substitution of Zn by Fe, Cd, Mn, and Hg has been considered relevant, the sum of the remaining metal cations (Tables 3 and 4) usually being less than 0.1 at% (copper is considered separately in the following section). In Figure 2, a plot of at% Zn vs. at% (Fe + Mn + Cd + Hg) is shown for each point analysis. A linear correlation is clearly evident, i.e. a decrease in the Zn-content is matched

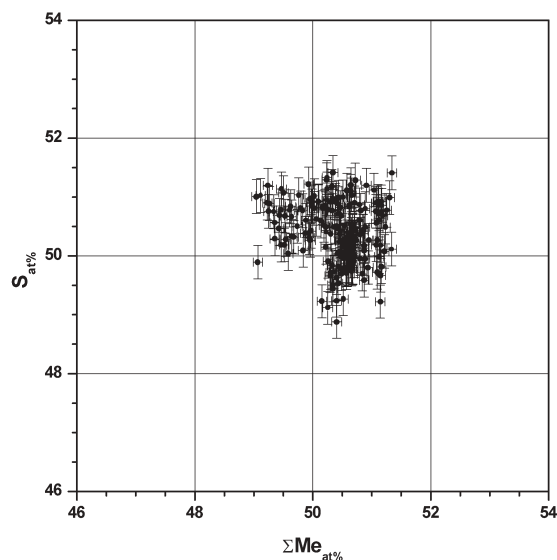


FIGURE 1. A plot of total metals (at% ΣMe) vs. sulfur (at% S) for all analytical points. $\Sigma\text{Me} = (\text{Zn} + \text{Fe} + \text{Mn} + \text{Cd} + \text{Hg} + \text{Cu})$.

TABLE 1. Provenance of the investigated samples

Sample	Provenance	Ore deposit type
1	Picos D'Europa, Spain	Cu-Au skarns
1164	Ingortosu (CA), Sardegna, Italy	hydrothermal Pb-Zn veins in "granitic" aureoles
1165 bis	Sarrabus, S. Vito, Casteddu, Sardegna, Italy	hydrothermal Pb-Zn veins in "granitic" aureoles
1168	Linares, Spain	hydrothermal Pb-Zn veins in "granitic" aureoles
1188	Lautenthal, Hartz, Germany	hydrothermal Pb-Zn veins in "granitic" aureoles
1189	Clausthal, Hartz, Germany	hydrothermal Pb-Zn veins in "granitic" aureoles
1206	Temeswar, Banato, Romania	Pb-Zn-Cu skarns
1210	Temeswar, Banato, Romania	Pb-Zn-Cu skarns
1211	Temeswar, Banato, Romania	Pb-Zn-Cu skarns
1212	Kapnik, Transilvania, Romania	epithermal Pb-Zn-Cu(AuAg) veins
1215	Kapnik, Transilvania, Romania	epithermal Pb-Zn-Cu(AuAg) veins
1227	Kapnik, Transilvania, Romania	epithermal Pb-Zn-Cu(AuAg) veins
1257	Kremnitz, Repubblica Slovakia	epithermal Pb-Zn-Cu(AuAg) veins
1276	Campiglia Marittima (LI), Toscana, Italy	Pb-Zn(Sn) skarns
1293	Ingortosu (CA), Sardegna, Italy	hydrothermal Pb-Zn veins in "granitic" aureoles
1303	Ingortosu (CA), Sardegna, Italy	hydrothermal Pb-Zn veins in "granitic" aureoles
1309	unknown	
47975	Elmwood, Tennessee	Zn-Pb MVT deposits
22551	Timmins, Ontario	Volcanic Massive Sulphide deposit
SPEH1	unknown	

by an increase in the amount of the other divalent cations. The total sum of cations replaces a corresponding amount of Zn, within experimental error, as evidenced by the linear regression parameters (see Fig. 2), confirming that significant contributions from other elements have not been neglected, and that a substitutional mechanism whereby divalent cations replace Zn in the tetrahedral sites, is observed.

The range of minor-element (Fe, Mn, and Cd) contents is fairly large for each sample (Table 3). Whereas the Fe-content may extend up to $2.5 \times$ the relative mean value (e.g., sample 1215), Cd and Mn ranges are lower, but still significant as shown by samples 1188 and 1165 bis, respectively. The variation of the cation contents, corresponding to their areal zoning, provides consistent limits to the accuracy and reliability of the bulk-chemical composition evaluated by averaging the single point analyses. As a consequence, correlations between the different elements (Fig. 3; see also Fig. 5) were derived taking into account

just the point analyses.

The plot of Hg vs. Mn (Fig. 3a) shows Mn to be present only in Hg-free areas. The plot of Hg vs. Fe, on the other hand, indicates that these metals occur together only below 0.03 at% HgS and 2 at% FeS, respectively (Fig 3b). On the basis of the trend in Figure 3a, the Hg-free (Mn-bearing) and Hg-bearing (Mn-free) point analyses were considered separately when the multiple correlations with Cd, Fe, and Mn were plotted in Figures 4a and 4b.

Considering the pseudoternary diagram presented in Figure 4a, Cd for Zn replacement is not substantially affected by the simultaneous presence of Fe and/or Mn, a result similar to that for the Zn-(Fe + Hg)-Cd pseudoternary system. CdS contents

TABLE 2. X-ray Lines, crystals and detection limits for the analysed elements

Line	Crystal	Element	Detection limit(ppm)
K _α	PET	S	0.05*
	LLIF	Zn	0.03*
K _α	PET	Ti	21
	LLIF	V	14
		Cr	13
		Mn	13
		Fe	16
		Co	12
		Ni	11
		Cu	30
		Ga	71
		As	35
L _α	TAP	Ge	174
		Se	125
	PET	Cd	130
		In	35
		Sn	72
M _α	PET	Hg	286

* Detection limits for major elements, obtained with different operating conditions, are expressed as wt%.

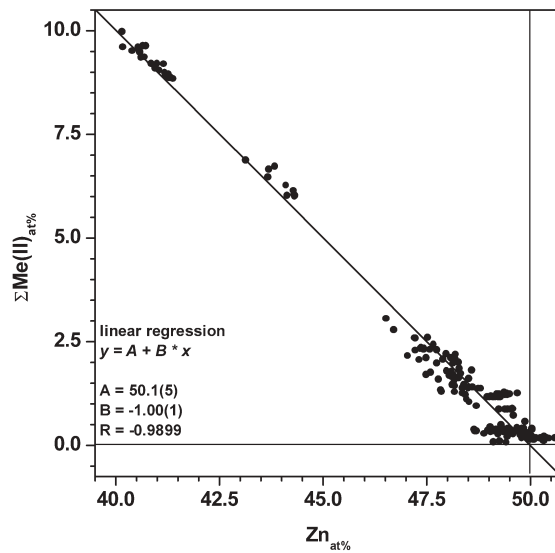


FIGURE 2. Total divalent metals [at% $\Sigma\text{Me}^{(2+)}$] vs. zinc (at% Zn) plot for all analytical points. $\Sigma\text{Me}^{(2+)} = (\text{Fe} + \text{Mn} + \text{Cd} + \text{Hg})$.

TABLE 3. Mean values for major and minor elements and totals (wt%)

Sample	Major		Minor								Tot		
	S	Zn	Fe		Mn		Cd		Cu			Hg	
			Mean	Range	Mean	Range	Mean	Range	Mean	Range		Mean	Range
1	31.72(18)	65.64(10)	0.144(2)	0.143-0.148	tr	/	0.081(8)	0.100-0.070	tr	/	tr	/	97.73(39)
1164	32.57(18)	65.20(10)	0.300(2)	0.362-0.349	tr	/	0.227(9)	0.352-0.195	tr	/	tr	/	98.52(22)
1165 bis	32.57(18)	54.48(9)	10.19(1)	10.90-9.644	0.215(2)	0.349-0.128	0.313(7)	0.344-0.243	tr	/	nd	/	97.91(31)
1168	32.15(18)	66.09(10)	0.046(1)	0.061-0.038	tr	/	0.099(8)	0.125-0.077	<mdl	/	0.21(2)	0.26-0.16	98.64(39)
1188	32.42(18)	62.51(9)	1.690(4)	2.599-0.382	tr	/	0.477(10)	0.876-0.171	0.110(2)	0.347-0.024	nd	/	97.35(21)
1189	32.63(18)	63.63(9)	1.564(4)	1.781-1.226	tr	/	0.315(9)	0.416-0.215	tr	/	tr	/	98.47(25)
1206	32.41(18)	64.69(10)	0.227(2)	0.255-0.185	tr	/	0.350(10)	0.417-0.270	tr	/	<mdl	/	97.81(39)
1210	32.22(18)	63.63(9)	1.885(4)	2.154-1.556	tr	/	0.570(10)	0.705-0.456	tr	/	tr	/	98.50(44)
1211	32.15(18)	58.00(9)	6.319(9)	6.989-5.961	0.589(3)	0.660-0.567	0.432(10)	0.455-0.419	tr	/	nd	/	97.77(41)
1212	32.49(18)	64.00(9)	0.290(2)	0.309-0.249	1.342(4)	1.858-1.067	0.354(10)	0.379-0.322	tr	/	nd	/	98.52(35)
1215	32.72(18)	63.65(9)	1.359(3)	3.388-0.016	tr	/	0.143(9)	0.183-0.103	tr	/	nd	/	97.95(37)
1227	31.97(18)	65.20(10)	0.284(1)	0.294-0.277	0.887(2)	0.911-0.871	0.444(7)	0.459-0.424	tr	/	nd	/	98.82(30)
1257	31.89(18)	64.82(10)	0.353(2)	0.393-0.203	0.362(2)	0.882-0.233	0.411(10)	0.454-0.388	tr	/	nd	/	97.90(36)
1276	32.57(18)	62.86(9)	2.335(5)	2.533-2.242	0.293(2)	0.320-0.281	0.154(9)	0.176-0.133	tr	/	nd	/	98.34(41)
1293	32.29(18)	64.39(9)	0.266(2)	0.314-0.230	tr	/	0.255(9)	0.292-0.230	tr	/	tr	/	97.36(39)
1303	32.05(18)	64.59(10)	1.151(3)	1.158-1.141	tr	/	0.322(9)	0.341-0.306	tr	/	nd	/	98.21(39)
1309	32.50(18)	64.87(10)	0.235(2)	0.294-0.190	tr	/	0.296(9)	0.341-0.247	tr	/	nd	/	98.02(39)
22551	32.46(17)	59.55(9)	9.508(8)	10.62-6.590	0.420(2)	0.771-0.006	0.331(6)	0.389-0.249	<mdl	/	nd	/	98.98(29)
47975	32.24(18)	65.74(10)	0.218(1)	0.312-0.161	tr	/	0.113(6)	0.348-0.167	<mdl	/	nd	/	98.37(30)
SPEH1	33.06(17)	54.56(8)	6.328(1)	10.58-0.161	0.185(2)	0.786-0.001	0.267(7)	0.379-0.080	tr	/	nd	/	99.19(29)

Notes: Compositional range for minor elements. Contents indicated as "tr" are reported in Table 4. In brackets are reported the standard deviations. nd = not detected.

TABLE 4. Mean values for trace elements (ppm)

Sample	Mn	Ti	V	Cr	Co	Cu	Hg	In	As	Se
1	31(17)	65(24)	34(20)	28(18)	<mdl	72(19)	329(227)	140(39)	<mdl	<mdl
1164	39(18)	96(24)	39(20)	41(18)	<mdl	85(20)	411(223)	111(39)	<mdl	<mdl
1165 bis	Minor	60(17)	35(14)	31(13)	nd	436(14)	nd	751(40)	<mdl	69(48)
1168	42(18)	95(24)	39(20)	35(18)	nd	<mdl	Minor	129(39)	<mdl	<mdl
1188	68(18)	51(24)	35(20)	25(18)	46(14)	Minor	nd	134(39)	49(32)	<mdl
1189	57(18)	104(24)	43(20)	35(18)	15(14)	604(20)	707(225)	142(39)	<mdl	<mdl
1206	33(18)	99(24)	29(20)	32(18)	94(14)	103(19)	<mdl	130(39)	nd	<mdl
1210	84(18)	87(24)	27(18)	22(18)	nd	80(19)	498(222)	132(39)	<mdl	<mdl
1211	Minor	26(24)	29(19)	30(18)	nd	42(19)	nd	98(39)	<mdl	<mdl
1212	Minor	80(24)	38(20)	42(18)	<mdl	73(19)	nd	Nd	<mdl	nd
1215	51(18)	59(24)	33(20)	42(18)	nd	78(19)	nd	129(39)	nd	nd
1227	Minor	55(17)	33(14)	34(13)	8(10)	30(13)	nd	51(39)	<mdl	<mdl
1257	Minor	68(24)	40(20)	27(18)	<mdl	107(19)	nd	130(39)	<mdl	nd
1276	Minor	45(24)	35(22)	42(18)	nd	43(21)	nd	56(39)	nd	<mdl
1293	33(18)	89(24)	46(20)	30(18)	<mdl	339(19)	307(222)	142(39)	<mdl	<mdl
1303	43(18)	46(24)	40(20)	30(18)	<mdl	32(19)	nd	205(39)	<mdl	<mdl
1309	31(18)	61(24)	41(19)	34(18)	87(14)	190(19)	<mdl	133(39)	<mdl	<mdl
22551	75(13)	55(17)	38(14)	32(13)	nd	<mdl	nd	197(39)	nd	51(49)
47975	36(12)	63(17)	45(14)	35(13)	<mdl	211(14)	nd	118(39)	<mdl	<mdl
SPEH1	Minor	60(17)	29(14)	32(13)	nd	296(44)	nd	282(39)	<mdl	<mdl

Notes: Contents indicated as "minor" are reported in Table 3. In brackets are reported the standard deviations; nd=not detected.

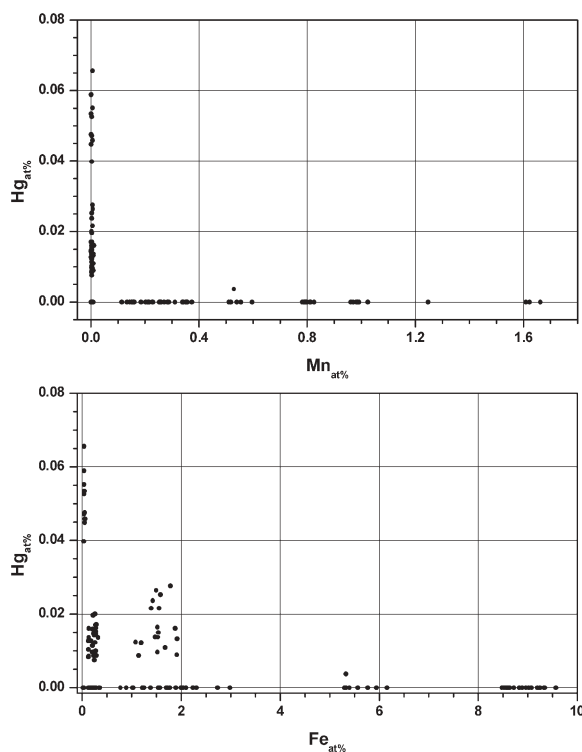


FIGURE 3. (a) Plots of manganese (at% Mn) vs. mercury (at% Hg) and (b) iron (at% Fe) vs. mercury (at% Hg).

may be considered, at least below 1.0 at%, as being independent of Fe-, Mn-, and Hg-concentrations. On the other hand, the concentration of Mn strongly depends on the Fe-content (Fig. 4b). The highest MnS concentrations (up to 4.0 at%) were found in samples with a (Fe + Cd) content below 2.0 at%, whereas less than 2.0 at% Mn was found in samples with a higher Fe concentration. The experimental data seem to show a limited compositional field (indicated by the continuous line in Fig. 4b), where coupled substitution of Fe and Mn for Zn may occur. Although these analyses were obtained from a limited number of samples, the results reflect the more general behavior of Mn

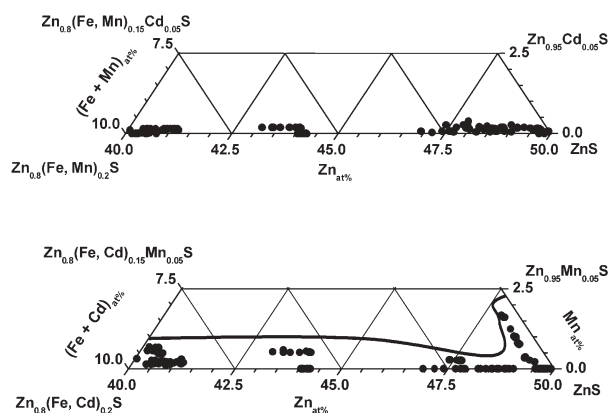


FIGURE 4. Pseudoternary diagrams for the minor elements in sphalerite (a) Zn - (Fe + Mn) - Cd and (b) (Zn + Cd) - (Fe) - Mn, expressed in at%. The continuous line defines the compositional field of the simultaneous presence of Mn and Fe.

and Fe partitioning in ZnS. Balakishieva (1964), studying 150 monomineralic sphalerite samples of different provenance, observed a direct correlation between Mn and Fe concentrations, although the compositional ranges presented by them for both elements are contained within the field shown in Figure 4b.

A plot of Cu vs. In is shown in Figure 5. A 1:1 linear trend, found for all In-contents, is evident. According to Johan (1988), this trend arises from local "roquesite-like" domains in the crystal. The uncorrelated Cu-rich analytical points falling below this linear trend (Fig. 5) appear to be distributed below the concentration limit for simple Cu-Zn substitution (Patrick et al. 1998). However, Cu is found to compete with Mn in replacing Zn, thus accumulating in the Fe-rich grains. A linear correlation between the Cu- and Fe-contents does not yield an adequate picture of Cu-Fe trends, hidden by a high Fe²⁺ fraction that is not correlated to the amount of Cu. The dimension of the electron beam used (~20 μm²) does not allow discrimination of sub-micrometer structures. Considering that Ga, Ge, and Sn were

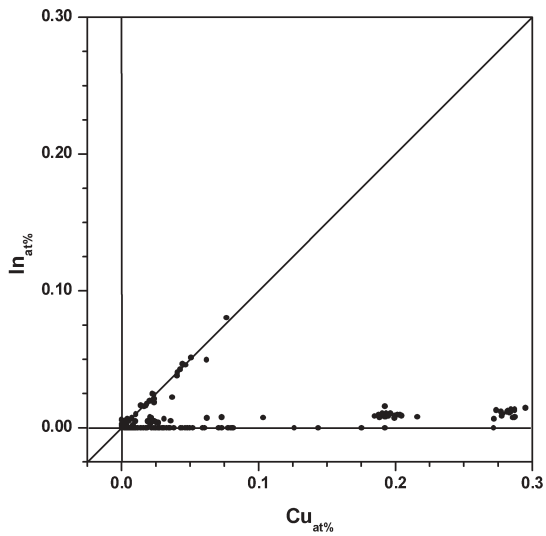


FIGURE 5. A plot of indium (at% In) vs. copper (at% Cu) concentrations. The diagonal line represents the “roquesite-like” composition.

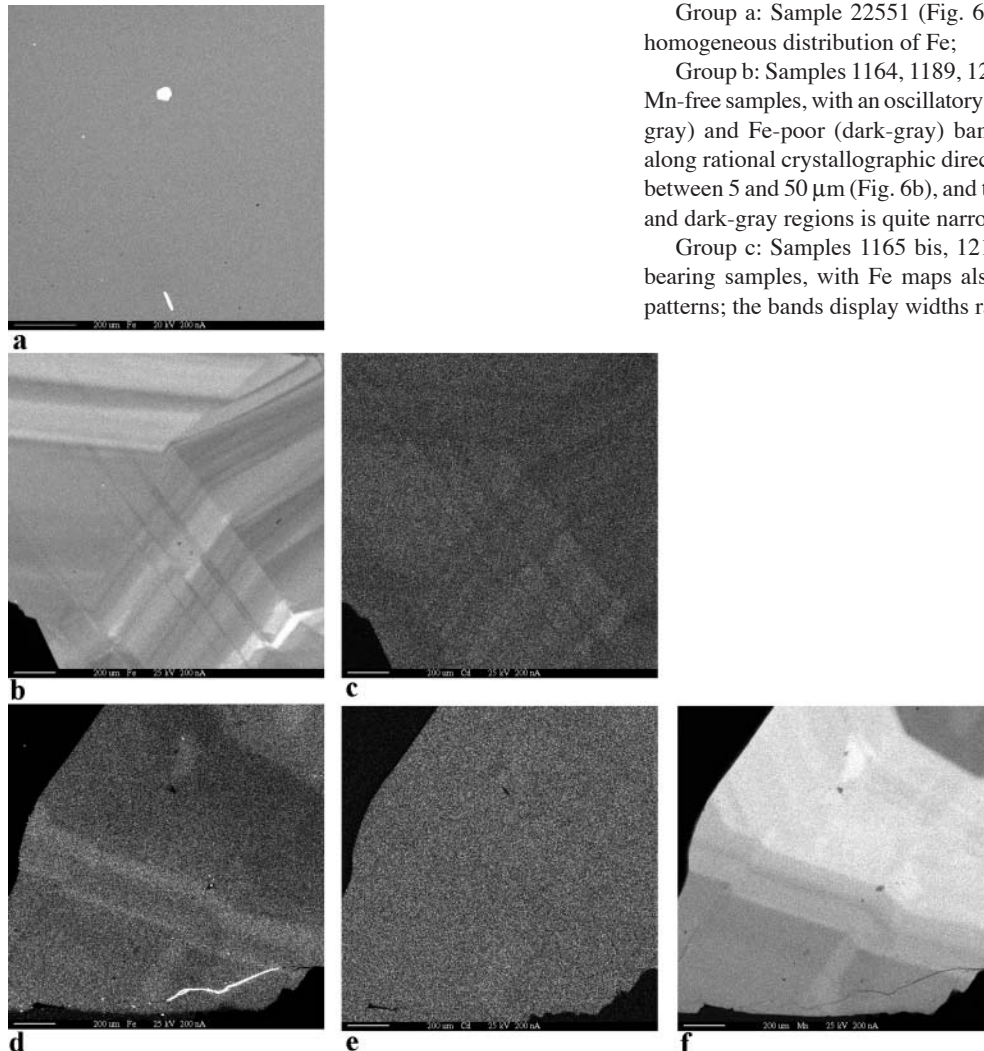


FIGURE 6. X-ray element distribution maps (a) Sample 22551 Fe map; (b) Fe and (c) Cd maps for sample 1210 (group b, as defined in the text); (d) Fe, (e) Cd, (f) Mn maps for sample 1212 (group c, as defined in the text). Lighter regions correspond to higher element contents.

not detected (see below), the occurrence of Cu in Fe-enriched grains suggests that Cu is involved preferentially in a coupled (Cu + Fe) substitutional mechanism, leading to chalcopyrite-like nano-domains (Johan 1988).

The mean values of the trace elements detected in the point analyses are reported in Table 4. Sporadic point analyses reveal the presence of Ni and Se, but no Ga, Ge, or Sn. The concentration of Co is always low (Hall 1961), even if these divalent ions are stable and present in the sulfide environment (Vaughan and Craig 1978). Co-Zn substitution, in fact, has been studied in synthetic sphalerites, with very high concentrations of Co being reported (up to 10 at%, Lawniczacz-Jablonska et al. 1994).

Distribution maps

Selected Fe, Cd, and Mn X-ray element distribution maps are shown in Figure 6. Samples 1164, 1189, 1206, 1210, 1215, 22551, and 47975 show no meaningful Mn distribution due to the small number of counts detected, in agreement with the results of the point analyses (Table 3). All of the Fe distribution maps, with the exception of that for sample 22551 (Fig. 6a), show obvious zoning. The investigated samples fall into three groups, in terms of Fe distribution patterns and Mn concentrations.

Group a: Sample 22551 (Fig. 6a). Mn-free sample, with a homogeneous distribution of Fe;

Group b: Samples 1164, 1189, 1206, 1210, 1215, and 47975. Mn-free samples, with an oscillatory alternation of Fe-rich (light-gray) and Fe-poor (dark-gray) bands, which appear oriented along rational crystallographic directions; the band widths vary between 5 and 50 μm (Fig. 6b), and the boundary between light- and dark-gray regions is quite narrow (1–5 μm);

Group c: Samples 1165 bis, 1211, 1212, and SPEH1. Mn-bearing samples, with Fe maps also characterized by banded patterns; the bands display widths ranging between 50 and 400

μm , with less well-defined boundaries (10–150 μm) among light (Fe-rich) and dark gray (Fe-poor) regions (Fig. 6d). The Mn maps of these samples reveal an antithetic inhomogeneous distribution; large Mn-rich bands (light gray in Fig. 6f) closely correspond to the Fe-poor regions (dark gray in Fig. 6d), and vice versa, in all samples of this group.

An inhomogeneous distribution of Cd was also observed in several of the maps. Cadmium is characterized by a homogeneous distribution in sample 22551 and in the samples of Group c (Fig. 6e). On the other hand, patterns of distribution that closely follow the corresponding Fe map are evident in the samples of Group b (Fig. 6c).

All the banded features observed in these distribution maps show an obvious compositional variation during the growth of all the faces of a crystal, i.e., concentric zoning. On the other hand, some features such as the small bands perpendicular to the growing face (at the bottoms of Figs. 6d and 6f) suggest the possible presence of sector zoning due to the non-centrosymmetric structure of sphalerite (Agrosi et al. 2002).

DISCUSSION

The data provided by the point analyses highlight the compositional inhomogeneity commonly found in sphalerite crystals. Craig and Vaughan (1994) describe sphalerite as the most refractory sulfide, potentially recording evidence for the conditions of its genesis. The observed zoning and cation distributions have to be, therefore, related to the precipitation process. The mechanism of sector zoning, i.e., the differential partitioning of an element among non-equivalent crystallographic faces, leads to the formation of observable “sectors.” The eventual variation of the composition of the mineralizing fluid results in different concentric bands in each sector. However, sector zoning is not responsible for the presence of concentric zones, even if the two structures are frequently associated (Vesselinov and Kerestodjic 1995; Agrosi et al. 2002). Concentric zoning, i.e., the alternation of different bands parallel to the same growing face is, in fact, related to the physico-chemical conditions of nutrient supply, both at the large- and small-scale. In the present samples, most of the observed zoning is a concentric alternation of bands with different compositions. As a consequence, this zoning may be explained by invoking variations in the fluid from which the sphalerite precipitates, but it may also reflect interactions among the minor elements. Several reports in the literature suggest a driving force in controlling isomorphic substitution: Furdyna (1988) and Twardowski (1990) found Mn^{2+} and Fe^{2+} to coalesce in nearest-neighbor sites in the sphalerite lattice giving rise to

long-range magnetic interactions.

In the Fe-Mn-(Zn + Cd) ternary diagram (shown in Fig. 7), the mean compositional data of Table 3 are plotted using symbols showing membership of Groups a, b, and c. Most of the Group b samples fall near to the (Zn + Cd) corner, their Fe contents varying from 0 to 4 at%, whereas sample 22551 is isolated at ~ 12 at% Fe. The Group c samples plot in both the Mn- and Fe-rich regions of the diagram. Considering the whole data set, it can be seen that samples of different provenance belonging to the same group (e.g., 1164, 1189, 1206, ...), as opposed to samples from the same locality but different groups (1210/1211 and 1212/1215), show markedly different patterns. Moreover, whereas the Group b samples occupy only a small compositional field relative to the observation of associated Fe and Cd patterns, the Group c distribution in the ternary diagram suggests Mn and Fe segregation unrelated to the bulk-chemical composition of the specimen. The banding pattern of the Fe and Mn maps for Group c, therefore, is neither dependent on sample provenance nor bulk-chemical composition. This finding cannot be easily explained in terms of variation of the chemical composition of the fluid. The metal zoning may be related to competition between Fe and Mn due to limited reciprocal affinity, the two ions exerting surface chemical control during the absorption process.

The tendency of both Fe and Mn to form homonuclear clusters in adjacent sites in sphalerite, which may be considered as a precursor of the observed zoning, has been discussed extensively in the literature (Gerard et al. 1971; Furdyna 1988; Twardowski et al. 1988; Balabin and Sack 2000; Bernardini et al. 2004; Di Benedetto 2003). Several properties (ionic radius, crystal-field-stabilization energy, nature and strength of the magnetic interaction), all of which differ between Fe and Mn, play an important role in establishing the distribution of ions during crystal growth: Fe and Mn pairs in adjacent sites and larger clusters have been identified in both natural and synthetic sphalerite (Gerard et al. 1971; Kreissl and Gehlhoff 1984; Bernardini et al. 2004). Moreover, the existence of clustering (from nano- to microscopic scale) of paramagnetic solute ions in ZnS has been proposed on the basis of theoretical studies by Twardowski et al. (1988) and Balabin and Sack (2000). Both these authors showed, in agreement with Furdyna (1988), that specific Fe-Fe and Mn-Mn interactions are the origin of the observed local and/or short-range ordering that drives the entire crystallization process. Neutron diffraction, magnetization, and EPR studies (Spalek et al. 1986; Furdyna 1988; Twardowski 1990) have contributed to demonstrating that the low-temperature magnetic behavior (e.g., magnetic susceptibility, EPR line width) of Mn- and Fe-bearing sphalerites is determined by an inhomogeneous distribution of cations, and by a long-range antiferromagnetic interaction that correlates ions beyond the first cationic coordination shell. The competition between Fe and Mn in substituting for Zn appears, therefore, to be driven by a “chemical” control at the crystal-fluid interface, causing their incorporation into sphalerite in different regions and at different times. At least in some cases, the ore formation conditions exert only a minor control on crystal zoning. Due to their competing behavior, when the solid becomes enriched in Fe(Mn), the Mn(Fe) accumulates in the fluid near to the mineral surface. Only after consumption of the excess of the first ion, does the second ion start to be chemisorbed. The

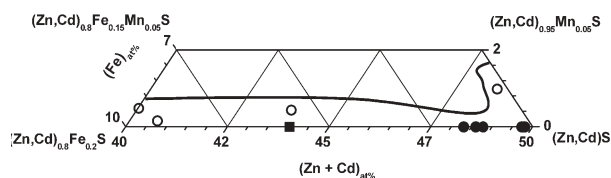


FIGURE 7. Part of the ternary diagram (Zn + Cd)-Fe-Mn, expressed in atom%. The continuous line defines the limits noted in Figure 4b; the filled squares, filled circles, and open circles are the mean chemical compositions (Table 1) of samples from groups a, b, and c, respectively, as defined in the text.

poorly defined boundary between Fe-rich and Mn-rich regions in Group c crystals may be explained in terms of the small field of simultaneous concentration (Di Benedetto et al. 2003).

As regards the distribution of Cd, which can readily substitute for Zn in the sphalerite structure despite its different ionic size (Patrick et al. 1998), a homogeneous distribution is characteristic of all Group c samples. Because slow crystallization favors homogeneous absorption, the Cd distribution in Group c samples may indicate a growth rate slow enough to allow Cd to be chemisorbed homogeneously. The decrease of the growth rate is in agreement with the competition between Mn and Fe. On the other hand, the overall process, chemically controlled at the front of crystallization, appears to be faster than any eventual external variation of the component supply (Katsev and L'Heureux 2001).

The oscillatory zoning of Fe and Cd in Mn-free samples, as in Group b, is more difficult to explain; no obvious chemical constraints can be invoked to suggest the presence of an interface control of crystal growth. According to Holten et al. (1997), the very low solute (Fe + Cd) content allows both externally and internally controlled crystal growth. Chemisorption may control an oscillatory crystallization if an effectively stationary regime regarding the supply of components is established. Katsev and L'Heureux (2001), studying a Mississippi Valley Type sphalerite sample, demonstrated a self-organized compositional pattern and showed that an internal control of zoning may be $\sim 10^4$ times faster than any external control. The overall compositions of the Mn-free samples, which plot near to the Zn corner of the ternary diagram whatever their provenance (Fig. 4), suggest that the banding is the result of an internally controlled process.

All of the experimental data reflect a complex situation, where surface dependent processes, and processes related to the thermodynamics of complex species, or variations in the mineralizing fluid, may occur. The mutual interactions between Zn and the minor- or trace-element substituents, and those among the minor or trace elements themselves, may provide a significant contribution to the uptake and distribution of dopants in sphalerite. Our point analyses suggest that the Co-, Ni-, and Hg- concentrations in sphalerite are affected, as is the Mn-content, by the presence of Fe, but the main limitation to their concentrations can be ascribed to the larger scale geochemical association (e.g., Dobrovolskaya and Belyayev 1989). The magnetic interactions induced by the presence of paramagnetic Fe may be responsible for the low concentration of Co^{2+} in the investigated natural sphalerites, due to the different paramagnetic properties of this d^7 ion. Nickel, on the other hand, occurs preferentially in sixfold coordination in sulfides (pyrrhotites, vaesite, thiospinels; e.g., Putnis 1991). The larger crystal-field-stabilization energy, characteristic of octahedral coordination (Greenwood and Earnshaw 1992), may contribute to limiting the concentration of Ni in sphalerites, where only tetrahedral sites are available (Czamanske and Goff 1973). Nevertheless, these authors have pointed out the mutual influence between Fe and Ni substituting for Zn in sphalerite. A different thermodynamic stabilization of the paramagnetic ions (Fe, Mn) in the regions locally enriched in diamagnetic substituent elements (especially Hg) may be responsible for their significant partitioning (e.g., Furdyna 1988). The different character of the Hg-S bond (as seen

both in cinnabar and metacinnabar), compared to the (Zn, Cd)-S bonds, the covalence and electron delocalization of which are greater (Greenwood and Earnshaw 1992), may affect the super-exchange interaction observed for Mn and Fe, which is sensitive to the nature of the anionic p-orbital involved (Twardowski 1990; Furdyna 1988).

CONCLUDING REMARKS

An exact knowledge of chemical composition and metal distribution is of fundamental importance to the characterization of sphalerite-based semiconductors. The mean concentration values obtained by microanalysis must be considered very carefully, particularly for large crystals. The simultaneous replacement of Zn by Mn and Fe (and rarely Cd) may prevent an accurate determination of bulk-chemical composition. This problem may be overcome by using measurements of the lattice constant provided by XRD investigations of powdered crystals, as suggested by Furdyna (1988).

Inhomogeneous distribution of Fe, Mn, and Cd, substituting for Zn, has been identified both in Mn-free samples with a low Fe-content, and in Mn-bearing samples. In the presence of Mn, the zoning patterns may be related to the limited coupled concentration of Fe and Mn in sphalerite. Generally, any crystallization process is slow, allowing the separation of these two ions to occur and allowing the homogeneous precipitation of Cd.

The Fe-Cd bands observed in Mn-free samples suggest a crystal growth mechanism controlled mainly at a local scale [i.e., a self-organized solute (Fe, Cd) deposition via a fast feedback process]. According to this model, the fluctuations of the component supply induce only a minor perturbation of the process, as reported in Katsev and L'Heureux (2001). Nevertheless, an external origin (Holten et al. 1997) cannot be eliminated completely.

The fundamental role played during crystallization by the low affinity between Mn and Fe shows the importance of processes at and near the crystal surface in sphalerite, confirming that this mineral can provide a record of non-linear depositional processes.

ACKNOWLEDGMENTS

This manuscript benefited from careful and detailed reviews by P. Barton and S.D. Scott, which are sincerely acknowledged. This work was undertaken when the first author (F.D.B.) was a Visiting Fellow at the University of Manchester (Williamson Research Centre) Marie Curie Training Site, and the European Commission is thanked for funding this visit. The NERC and EPSRC are also thanked for funding equipment at the Williamson Research Centre. This research was also co-financed by the COFIN01 and COFIN03 research funds by Italian MIUR.

REFERENCES CITED

- Agrosi, G., Schingaro, E., Pedrazzi, G., Scandale, E., and Scordari, F. (2002) A crystal chemical insight into sector zoning of a titanian andradite ('melanite') crystal. *European Journal of Mineralogy*, 14, 785–794.
- Ancey, M., Bastenaire, F., and Tixier, R. (1980) *Microanalysis and Scanning Electron Microscopy Summer School* (St. Martin d'Hères, 38041 France), 330 p. Les Editions de Physique, Orsay, France
- Axelsson, M.D. and Rodushkin, I. (2001) Determination of major and trace elements in sphalerite using laser ablation double focusing sector field ICP-MS. *Journal of Geochemical Exploration*, 72, 81–89.
- Balabin, A.I. and Sack, R.O. (2000) Thermodynamics of (Zn, Fe)S sphalerite. A CVM approach with large basis clusters. *Mineralogical Magazine*, 64, 923–943.
- Balabin, A.I. and Urusov, V.S. (1995) Recalibration of the sphalerite cosmobarometer: experimental and theoretical treatment. *Geochimica et Cosmochimica Acta*, 59, 1401–1410.
- Balakishieva, B.A. (1964) Geochemistry of cadmium, manganese and iron in sphalerites. *Izvestiä Akademii Nauk Azerbajdzanskoj SSR, Ser. Geol.-Geogr.*

- Nauk, 6, 27–34
- Barton, P.B. and Toulmin, P., III (1966) Phase relations involving in the Fe-Zn-S system. *Economic Geology*, 61, 815–849.
- Bente, K. (1987) Stabilisation of Cu-Fe-Bi-Pb-Sn-sulfides. *Mineralogy and Petrology*, 36, 205–217.
- Bernardini, G.P., Borgheresi, M., Cipriani, C., Di Benedetto, F. and Romanelli, M. (2004) Mn distribution in sphalerite an EPR study. *Physics and Chemistry of Minerals*, 31, 80–84.
- Bjørkum, P.A. and Walderhaug, O. (1990) Geometrical arrangement of calcite cementation within shallow marine sandstones. *Earth Science Reviews*, 29, 145–161.
- Chadam, J. and Ortoleva, P. (1990) Morphological instabilities in physico-chemical systems. *Earth Science Reviews*, 29, 175–181.
- Cook, N.J. (1996) Mineralogy of the sulphide deposits at Sulitjelma, northern Norway. *Ore Geology Reviews*, 11, 303–338.
- Craig, J.R. and Vaughan, D.J. (1994) *Ore microscopy and ore petrography*, 434 p. Wiley, New York.
- Czamaske, G.K. and Goff, F.E. (1973) The character of Ni²⁺ as demonstrated by solid solutions in the Ni-Fe-Zn-S system. *Economic Geology*, 68, 258–268.
- Dewers, T. and Ortoleva, P. (1994) Nonlinear dynamical aspects of deep basin hydrology fluid compartment formation and episodic fluid release. *American Journal of Science*, 294, 713–755.
- Di Benedetto, F. (2003) Indagini minero-chimiche e spettroscopiche su sfaleriti naturali e analoghi sintetici. Ph.D. thesis, 154 p. University of Florence, Italy.
- Di Benedetto, F., Bernardini, G.P., Caneschi, A., Cipriani, C., Danti, C., Pardi, L., and Romanelli, M. (2002) EPR and magnetic investigations on sulphides and sulphosalts. *European Journal of Mineralogy*, 14, 1053–1060.
- Di Benedetto, F., Bernardini, G.P., Cipriani, C., Plant, D., Romanelli, M., and Vaughan, D.J. (2003) Mn distribution in natural sphalerites, a microanalytical and EPR study. *Geophysical Research Abstracts*, 5, 13985.
- Dobrovolskaya, M.G. and Belyayev, A., Yu. (1989) Associations of trace elements in sphalerite as indicators of the associational and genetic types of Lead-Zinc deposits. *Doklady Akademii Nauk SSSR*, 306, 969–972.
- Fialin, M., Rémy, H., Richard, C. and Wagner, C. (1999) Trace element analysis with the electron microprobe. New data and perspectives. *American Mineralogist*, 84, 70–77.
- Furdyna, J.K. (1988) Diluted magnetic semiconductors. *Journal of Applied Physics*, 64, R29–R64.
- Gerard, A., Imbert, P., Prange, H., Varret, F., and Wintenberger, M. (1971) Fe²⁺ impurities, isolated and in pairs, in ZnS and CdS studied by the Mössbauer effect. *Journal of Physics and Chemistry of Solids*, 32, 2091–2100.
- Greenwood, N.N. and Earnshaw, A. (1992) *Chimica degli elementi*. Piccin (Padova), 2, 731–1582.
- Hall, W.E. (1961) Unit cell edges of cobalt- and cobalt-iron-bearing sphalerites. U.S. Geological Survey Prof. Paper 424-B, 271–273.
- Holten, T., Jamtveit, B. and Meakin, P. (2000) Noise and oscillatory zoning of minerals. *Geochimica et Cosmochimica Acta*, 11, 1893–1904.
- Holten, T., Jamtveit, B., Meakin, P., Cortini, M., Blundy, J. and Austrheim, H. (1997) Statistical characteristics and origin of oscillatory zoning in crystals. *American Mineralogist*, 82, 596–606.
- Huston, D.L., Sie, S.H., Suter, G.F., Crooke, D.R., and Both, R.A. (1995) Trace elements in sulfide minerals from eastern Australian volcanic hosted massive sulfide deposits. Part I proton microprobe analyses of pyrite, chalcocopyrite and sphalerite and Part II Selenium levels in pyrite comparison with $\delta^{34}\text{S}$ values and implications for the source of sulfur in volcanogenic hydrothermal systems. *Economic Geology*, 90, 1167–1196.
- Hutchison, M.N. and Scott, S.D. (1981) Sphalerite geobarometry in the Cu-Fe-Zn-S system. *Economic Geology*, 76, 143–153.
- Johan, Z. (1988) Indium and germanium in the structure of sphalerite an example of coupled substitution with copper. *Mineralogy and Petrology*, 39, 211–229.
- Katsev, S. and L'Heureux, I. (2001) Two-dimensional model of banding pattern formation in minerals by means of coarsening waves Mississippi Valley-type sphalerite. *Physics Letters A*, 292, 66–74.
- Kieft, K. and Damman, A.H. (1990) In-bearing chalcocopyrite and sphalerite from the Gåsborn area, West Bergslagen, central Sweden. *Mineralogical Magazine*, 54, 109–112.
- Kojonen, K. and Johansson, B. (1999) Determination of refractory gold distribution by microanalysis, diagnostic leaching and image analysis. *Mineralogy Petrology*, 67, 1–19.
- Kreissl, J. and Gehlhoff, W. (1984) EPR investigations of ZnS:Mn and ZnSe:Mn. *Physica Status Solidi A*, 81, 701–707.
- L'Heureux, I. (1993) Oscillatory zoning in crystal growth a constitutional undercooling mechanism. *Physical Review E*, 48, 4460–4469.
- — — (2000) Origin of banded patterns in natural sphalerite. *Physical Review E*, 62, 3234–3245.
- L'Heureux, I. and Jamtveit, B. (2002) A model for oscillatory zoning in solid solutions grown from aqueous solutions: applications to the (Ba,Sr)SO₄ system. *Geochimica et Cosmochimica Acta*, 66, 417–429.
- Lawniczak-Jablonska, K., Golacki, Z., Paszkowicz, W., Masek, J., Johansson, L.S., and Heinonen, M. (1994) XPS studies of the Zn_{1-x}Co_xS electronic structure. *Journal of Physics: Condensed Matter*, 6, 3369–3378.
- Lepetit, P., Bente, K., Doering, T., and Luckhaus, S. (2003) Crystal chemistry of Fe-containing sphalerites. *Physics and Chemistry of Minerals*, 30, 185–191.
- Maurel, C. (1978) Stabilité de la blende dans le système Zn-Cd-S. *Bulletin de Minéralogie*, 101, 406–411.
- Oen, I.S., Kager, P., and Kieft, C. (1980) Oscillatory zoning of a discontinuous solid-solution series sphalerite-stannite. *American Mineralogist*, 65, 1220–1232.
- Ortoleva, P.J. (1990) Role of attachment kinetic feedback in the oscillatory zoning of crystal grown from melts. *Earth Science Reviews*, 29, 3–8.
- Patrick, R.A.D., Dorling, M., and Polya, D.A. (1993) TEM study of Indium- and Copper-bearing growth-banded sphalerite. *Canadian Mineralogist*, 31, 105–117.
- Patrick, R.A.D., Mosselmans, J.F.W., and Charnock, J.M. (1998) An X-ray absorption study of doped sphalerites. *European Journal of Mineralogy*, 10, 239–249.
- Prigogine, I. (1997) Non-linear science and the laws of nature. *Journal of the Franklin Institute*, 334B, 745–758.
- Putnis, A. (1991) *Introduction to mineral sciences*, 457 p. Cambridge University Press, U.K.
- Rager, H., Amthauer, G., Bernroder, M., and Schürmann, K. (1996) Colour, crystal chemistry and mineral association of a green sphalerite from Steiperf, Dill syncline, FRG. *European Journal of Mineralogy*, 8, 1191–1198.
- Reeder R.J., Fagioli, R.O., and Meyers, W.J. (1990) Oscillatory zoning of Mn in solution-grown calcite crystals. *Earth Science Reviews*, 29, 39–46.
- Roedder, E. and Dwornik, E.J. (1968) Sphalerite color banding lack of correlation with iron content, Pine Point, Northwest Territories, Canada. *American Mineralogist*, 53, 1523–1529.
- Scott, S.D. (1973) Experimental calibration of the sphalerite geobarometer. *Economic Geology*, 68, 466–474.
- Scott, S.D. and Barnes, H.L. (1972) Sphalerite-wurtzite equilibria and stoichiometry. *Geochimica et Cosmochimica Acta*, 36, 1275–1295.
- Shore, M. and Fowler, A.D. (1996) Oscillatory zoning in minerals a common phenomenon. *Canadian Mineralogist*, 34, 1111–1126.
- Spalek, J., Lewicki, A., Tarnawski, Z., Furdyna, J.K., Galazka, R.R., and Obuszko, Z. (1986) Magnetic susceptibility of semimagnetic semiconductors the high temperature regime and the role of superexchange. *Physical Review B*, 33, 3407–3418.
- Sultan, R., Ortoleva, P., DePasquale, F., and Tartaglia, P. (1990) Bifurcation of the Ostwald-Liesegang supersaturation-nucleation-depletion cycle. *Earth Science Reviews*, 29, 163–173.
- Tauson, V.L. and Chernyshev, L.V. (1977) Phase relationships and structural features of ZnS-CdS mixed crystals. *Geochemistry International*, 14, 11–22.
- Tauson, V.L., Chernyshev, L.V., and Makeyev, A.B. (1977) Phase relations and structural characteristics of mixed crystals in the system ZnS-MnS. *Geochemistry International*, 14, 33–45.
- Twardowski, A. (1990) Magnetic properties of Fe-based diluted magnetic semiconductors. *Journal of Applied Physics*, 67, 5108–5113.
- Twardowski, A., Swagten, H.J.M., van der Wetering, T.F.H., and de Jonge, W.J.M. (1988) Thermodynamic properties of iron-based II-VI semimagnetic semiconductors. *Solid State Communication*, 65(4), 235–239.
- Vaughan, D.J. and Craig, J.R. (1978) *Mineral chemistry of metal sulphides*, 494 p. Cambridge University Press, U.K.
- Vesselinov, I. and Kerestédjian, T. (1995) Kinetic aspects of sector zoning in arsenopyrite—a case study. *Mineralogy and Petrology*, 52, 85–106.
- Walgraef, D. (1990) Reaction-transport dynamics and dislocation patterns in deformed materials. *Earth Science Reviews*, 29, 299–308.
- Watson, E.B. and Liang, Y. (1995) A simple model for sector zoning in slowly grown crystals implications for growth rate and lattice diffusion, with emphasis on accessory minerals in crustal rocks. *American Mineralogist*, 80, 1179–1187.
- Wei, C. and Ortoleva, P. (1990) Reaction front fingering in carbonate-cemented sandstones. *Earth Science Reviews*, 29, 183–198.
- Wiggins, L.B. and Craig, J.R. (1980) Reconnaissance of the Cu-Fe-Zn-S system Sphalerite phase relationships. *Economic Geology*, 75, 742–751.

MANUSCRIPT RECEIVED JUNE 30, 2004

MANUSCRIPT ACCEPTED FEBRUARY 9, 2005

MANUSCRIPT HANDLED BY ALAN ANDERSON